

## The comparison of on-chip Surface Enhanced Raman Spectroscopy substrates: Nanoplasmonic bowtie antenna vs metal slot waveguide

A. Raza<sup>1,2</sup>, S. Clemmen<sup>1,2,3</sup>, M. V. Daele<sup>4</sup>, P. Wuytens<sup>1,2</sup>, J. Dendooven<sup>4</sup>, C. Detavernier<sup>4</sup> and R. Baets<sup>1,2</sup>

<sup>1</sup> Photonics Research Group, INTEC, Ghent University – imec, Belgium

<sup>2</sup> Center for Nano- and Biophotonics, Ghent University, Belgium

<sup>3</sup> Laboratoire d'information quantique, Université Libre de Bruxelles, 1050 Bruxelles, Belgium

<sup>4</sup> Department of Solid State Sciences, CoCooN Research Group, Krijgslaan 281/51, Ghent 9000, Belgium

*Surface enhanced Raman spectroscopy (SERS) is a widely known technique that exploits the highly localized plasmonic modes to probe the analyte in an ultra-small volume and concentration. Here, we present two different SERS substrates integrated on Si<sub>3</sub>N<sub>4</sub> platform i.e. localized surface plasmon resonance (LSPR) based bowtie antenna and surface plasmon polariton (SPP) based metal slot waveguide. Different performance parameters i.e. pump to Stokes conversion efficiency, broadband enhancement, structure size and ease of fabrication are discussed.*

Plasmonic nanostructures have attracted an immense attention in the recent years because of their remarkable ability to enhance dipole excitation and emission for the molecules lying in their hotspots. The ability of nanoplasmonics to manipulate the light at a level below the diffraction limit makes it an excellent platform for many sensing applications. Recently an advance step has been taken to integrate these plasmonic structures with the mature photonics technology that can eventually lead to a cheaper and miniaturized integrated sensor. Many sensing techniques i.e. on-chip LSPR [1], SERS [2-4] and SEIRA [5] has been demonstrated by integrating different plasmonic structures on a photonics waveguide. In this report, we compare the performance of two integrated SERS substrate i.e. nanoplasmonic bowtie antenna and metal slot waveguide. The performance parameters are as follows: pump to Stokes conversion efficiency, the broadband enhancement, structure size and the ease of fabrication.

First of all, the performance of both sensors in term of Stokes  $P_s$  to pump power  $P_o$  conversion efficiency ( $\eta$ ) is evaluated analytically using the figure of merit (FOM =  $P_s/P_o$ ) mentioned in [1] and [2]. A Lumerical 3D-FDTD software is used to simulate the hybrid modes of an antenna integrated on a waveguide. We assume a bowtie antenna integrated on a single mode Si<sub>3</sub>N<sub>4</sub> waveguide as shown in Fig 1. a. A 500  $\mu\text{m}$  linear taper is also introduced on the other side of antenna to avoid the back reflection of forward propagating Stokes signal and spurious Si<sub>3</sub>N<sub>4</sub> background. 1 nm thick 4-Nitrophenol is also applied on the gold surface to envision an analyte in the form of a monolayer. The design of the plasmonic antenna is chosen i.e. the antenna resonance matches well with the pump ( $\lambda_p = 785 \text{ nm}$ ) and Stokes wavelength ( $\lambda_s = 878 \text{ nm}$ ). This Stokes wavelength corresponds to the 1339  $\text{cm}^{-1}$  Raman mode of 4-Nitrophenol. Similarly, the FOM for a hybrid plasmonic waveguide is also calculated. The schematic of a plasmonic waveguide is depicted in Fig 1. b. An ALD Al<sub>2</sub>O<sub>3</sub> is used to reduce the gap of Si<sub>3</sub>N<sub>4</sub> slot waveguide fabricated using DUV lithography. The simulation results are shown in Fig 2. In the first set of simulations, we analyze the effect of the plasmonic gap on FOM. As shown in Fig 2. b, the FOM increases with decreasing the gap. This is attributed to high field enhancement in the plasmonic gap. For the case of a nanoplasmonic antenna, we

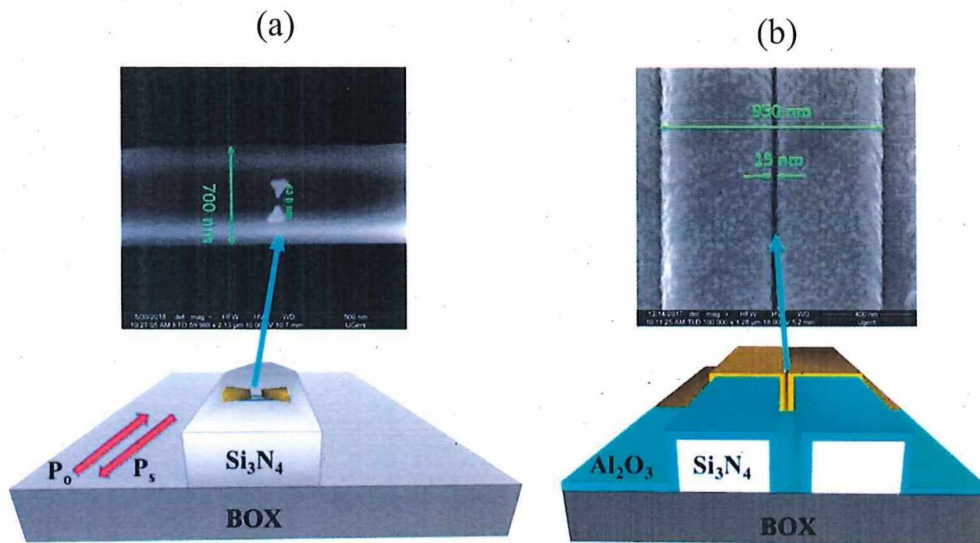


Fig 1. The schematic of the  $\text{Si}_3\text{N}_4$  integrated SERS sensors. a) The bowties antenna integrated a monomode  $\text{Si}_3\text{N}_4$  strip waveguide. b) The plasmonic waveguide interfaced with a monomode AlO clad  $\text{Si}_3\text{N}_4$  slot waveguide. The inset shows the SEM image of the fabricated sensor.

optimized the antenna geometry for each plasmonic gap i.e. the resonance wavelength ( $\lambda_R$ ) is always stays between pump and the Stokes wavelength. The FOM is calculated assuming an array of  $N=100$  antennas with a linear extinction of 1.3 dB each. Reducing the plasmonic gap from 50 nm to 10 nm, unlike the single molecule enhancement factor (SMEF), the FOM only increases 2 folds. This is due to an average enhancement over the whole antenna surface rather than over a single hot spot. For the plasmonic waveguide, we fix the  $\text{Al}_2\text{O}_3$  thickness to 50 nm and change the gold thickness i.e. the plasmonic gap sweeps from 50 nm to 10 nm. We also take a fixed plasmonic waveguide length of 50  $\mu\text{m}$  and 5 dB/facet photonics to plasmonic mode coupling efficiency. As shown in Fig 2. a, for a fixed gap = 10 nm, FOM for plasmonic waveguide is around  $50 \times$  larger than a nanoplasmonic antenna array. This is attributed to the microns long interaction length. The red and blue dotted lines in Fig 2. a, represents the final gap of the fabricated plasmonic waveguide and a nanoplasmonic antenna. It is worth mentioning that the final gap of the fabricated antenna is larger than the plasmonic waveguide gap but as confirmed from the Fig 2. a, this will hardly influence the enhancement gap between two sensors. In the second set of simulation, we analyze the effect of the interaction length in term of the number of antennas ( $N$ ) and plasmonic waveguide ( $L_p$ ). For a back scattered signal, the total Raman signal saturates after a certain number of antennas i.e.  $N=25$ . This is attributed to the decay of pump power due to an extinction of 1.3 dB offered by each nanoplasmonic plasmonic antenna. Similarly for a plasmonic waveguide, the FOM saturates after a specific waveguide length of 15  $\mu\text{m}$  due to the plasmonic waveguide loss ( $\approx 3 \text{ dB}/\mu\text{m}$ ).

Based on the above mentioned simulations, both SERS sensors are fabricated. The antennas on a waveguides are fabricated using two e-beam lithography steps. In the first step, the nanoplasmonic antenna array and the alignment markers were defined using a metal lift off. In the second step, the 700 nm wide  $\text{Si}_3\text{N}_4$  is fabricated. More fabrication details can be read from [1]. For the plasmonic waveguide, firstly, a  $\text{Si}_3\text{N}_4$  slot (150 nm) waveguide is fabricated using a 193 nm – DUV lithography. Then a 58 nm thick  $\text{Al}_2\text{O}_3$ , is conformally deposited using atomic layer deposition. This is followed by a contact lithography step to define the window for the plasmonic waveguide. Finally, the gold is sputtered over the chip followed by the metal lift off. Further fabrication details are



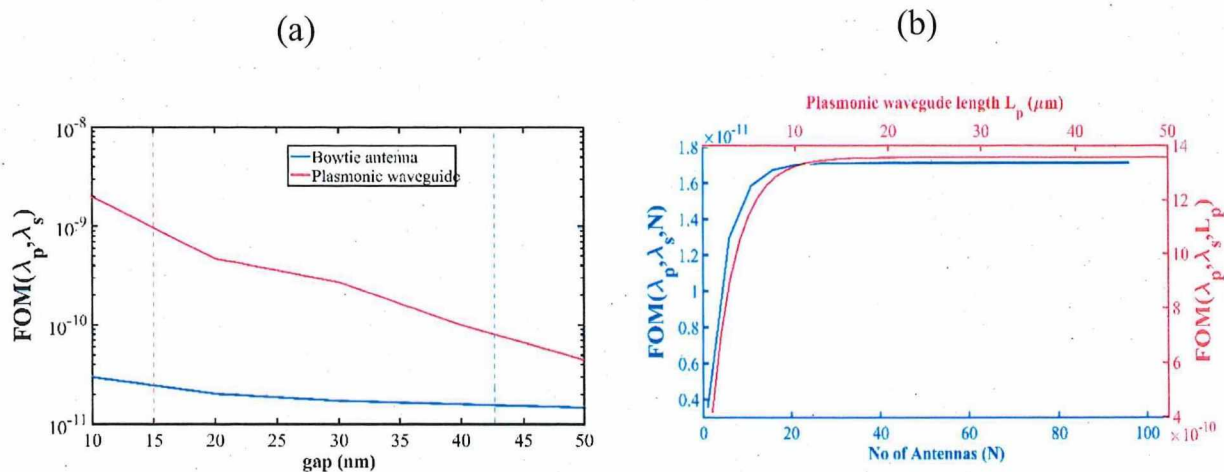


Fig 2. The calculated figure of merit (FOM) for a bowtie antenna (blue) and a plasmonic waveguide (red). a) The FOM as a function of plasmonic gap and b) interaction length (No of antennas for an antenna array and waveguide length for a plasmonic waveguide).

provided in [2]. In order to characterize the SERS sensors, a NTP monolayer is applied to the sensor by an overnight immersion in 1 mM solution of NTP in ethanol. The NTP monolayer selectively binds to the gold surface using Thiol-Au bond. After an NTP binding, the chips are cleaved in such a way the distance between waveguide facet and plasmonic structure is  $200 \mu\text{m}$ . The SERS measurements are done using a commercial confocal Raman microscope (WITEC Alpha300R+). A diode laser (Toptica XTRA II) lasing at 785 nm is used as a pump source. A high NA objective (100x/0.9 EC Epiplan NEOFLUAR;  $\infty/0$ ) is used for excitation and collection of the signal. Each spectra is recorded using 1 sec integration time. Further experimental details can be read from [2].

The measured Raman spectra are plotted in Fig 3. The pink dotted lines represent the NTP Raman peaks. A strong NTP signal is collected from a metal slot waveguide. However, in case of nanoantenna array, the NTP Raman spectrum is relatively weak. Along with NTP Raman modes, a broadband Raman background is also collected in the measured spectra that is attributed to the  $\text{Si}_3\text{N}_4$  background and photoluminescence of the gold. The plasmonic enhancement of a plasmonic antenna depends on the resonator quality factor (Q) and effective modal volume ( $V_{\text{eff}}$ ). Due to the high Q value and low

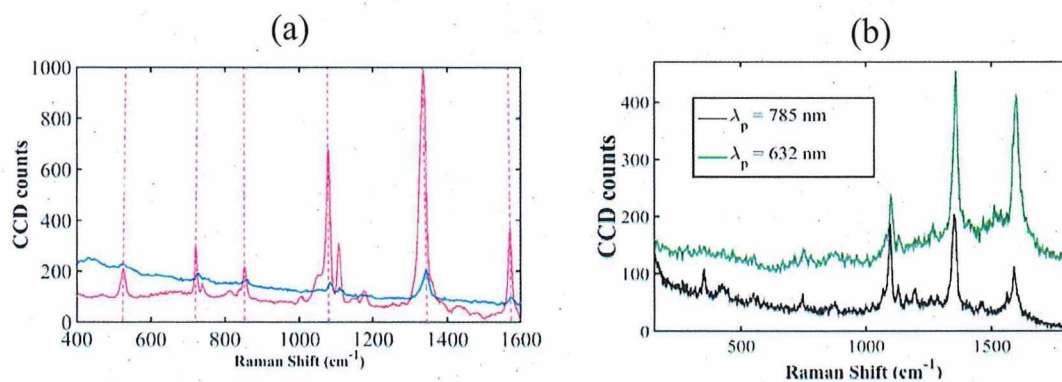


Fig 1. a) The Raman spectra of 4-Nitrophenol measured from a bowtie antenna (blue) and a metal slot waveguide (red) integrated with SiN waveguide. The pink dotted lines represent the Raman modes of NTP. b) The Raman spectra measured from a metal slot waveguide at 785 nm (black) and 632 nm (green) excitation wavelengths.

$V_{\text{eff}}$ , nanoantennas exhibits high field enhancement but it comes with the cost of low bandwidth e.g.  $\approx 200$  nm for bowtie antennas. However in the case of a plasmonic waveguide (gold-dielectric-gold waveguide), nonresonant enhancement of spontaneous emission rate scales with the wavelength in visible and NIR wavelength range [7] that makes the sensor structure independent of the excitation wavelength.. To verify this, SERS experiment on a metal slot waveguide is done using two different excitation wavelengths i.e. 632 nm and 785 nm. The results are shown in Fig 3. b. All the Raman modes of NTP can be seen in both spectra. The larger background in a 632 nm excited spectrum is attributed to the strong photoluminescence of the gold at lower wavelengths. Also, higher signal strength of NTP modes is due the wavelength dependent enhancement of the scattering cross section that scales with  $\approx \lambda^4$ .

In the conclusion, we have presented two different  $\text{Si}_3\text{N}_4$  waveguide interfaced SERS sensor i.e. an array of bowtie antenna and the metal slot waveguide. For a fixed plasmonic gap, metal slot waveguides exhibits strong Stokes to pump conversion efficiency. Also, the metal slot waveguide provides a broad band enhancement as compared to plasmonic bowtie antenna where the enhancement is limited to 200 nm wavelength range. The comparison of performance parameters for both devices are presented in Table. 1.

*Table 2. The comparison of a nanoplasmonic bowtie antenna and metal slot waveguide integrated on SiN platform in terms of the Stokes to Pumps conversion efficiency, broadband enhancement, structure size and fabrication.*

| Performance parameters       | Nanoplasmonic bowtie        | Metal slot waveguide            |
|------------------------------|-----------------------------|---------------------------------|
| $\eta$                       | $\approx 1 \times 10^{-12}$ | $\approx 1 \times 10^{-9}$      |
| Enhancement wavelength range | < 200 nm                    | broadband                       |
| Structure size               | $\approx 25$ antennas       | $\approx 15$ $\mu\text{m}$ long |
| fabrication                  | e-beam                      | ALD + DUV lithography           |

This research was funded by the ERC Grant InSpectra and FWO Belgium. Stephane Clemmen thanks the F.R.S-FNRS for financial support.

## References

- [1] M. Chamanzar, Z. Xia, S. Yegnanarayanan, and A. Adibi, "Hybrid integrated plasmonic-photonic waveguides for on-chip localized surface plasmon resonance (LSPR) sensing and spectroscopy," *Opt. Express* 21, 32086-32098 (2013).
- [2] F. Peyskens, A. Dhakal, P. Van Dorpe, N. Le Thomas, R. Baets, Surface Enhanced Raman Spectroscopy Using a Single Mode Nanophotonic-Plasmonic Platform, *ACS Photonics*, 3(1), p.102-108 (2016)
- [3] P.C. Wuytens, A.G. Skirtach, R. Baets, On-Chip Surface-Enhanced Raman Spectroscopy using Nanosphere-Lithography Patterned Antennas on Silicon Nitride Waveguides, *Optics Express*, 25(11), p.12926-12934 (2017)
- [4] A. Raza, M. Van Daele, P.C. Wuytens, J. Dendooven, C. Detavernier, S. Clemmen, R. Baets, "E-beam-lithography free plasmonic slot waveguides for on-chip Raman spectroscopy," in *Proceedings of the Conference CLEO 2018*, paper SW3L.6, 2018.
- [5] Q. Cao, J. Feng, H. Lu, H. Zhang, F. Zhang, and H. Zeng, "Surface-enhanced Raman scattering using nanoporous gold on suspended silicon nitride waveguides," *Opt. Express* 26, 24614-24620 (2018).
- [6] Che Chen, Daniel A. Mohr, Han-Kyu Choi, Daehan Yoo, Mo Li, and Sang-Hyun Oh, "Waveguide-Integrated Compact Plasmonic Resonators for On-Chip Mid-Infrared Laser Spectroscopy," *Nano Letters* Article ASAP DOI: 10.1021/acs.nanolett.8b03156
- [7] Y. C. Jun, R. D. Kekatpure, J. S. White, and M. L. Brongersma, "Nonresonant enhancement of spontaneous emission in 405 metal-dielectric-metal plasmon waveguide structures," *Phys. Rev. B* 78, 153111 (2008).